PERGAMON

International Journal of Solids and Structures 40 (2003) 3893–3911

INTERNATIONAL JOURNAL OF SOLIDS and STRUCTURES

www.elsevier.com/locate/ijsolstr

Axially compressed buckling of pressured multiwall carbon nanotubes

C.Y. Wang, C.Q. Ru *, A. Mioduchowski

Department of Mechanical Engineering, 4-9 Mechanical Engineering Bldg., University of Alberta, Edmonton, Alta., Canada T6G 2G8

Received 28 September 2002

Abstract

This paper studies axially compressed buckling of an individual multiwall carbon nanotube subjected to an internal or external radial pressure. The emphasis is placed on new physical phenomena due to combined axial stress and radial pressure. According to the radius-to-thickness ratio, multiwall carbon nanotubes discussed here are classified into three types: thin, thick, and (almost) solid. The critical axial stress and the buckling mode are calculated for various radial pressures, with detailed comparison to the classic results of singlelayer elastic shells under combined loadings. It is shown that the buckling mode associated with the minimum axial stress is determined uniquely for multiwall carbon nanotubes under combined axial stress and radial pressure, while it is not unique under pure axial stress. In particular, a thin N-wall nanotube (defined by the radius-to-thickness ratio larger than 5) is shown to be approximately equivalent to a singlelayer elastic shell whose effective bending stiffness and thickness are N times the effective bending stiffness and thickness of singlewall carbon nanotubes. Based on this result, an approximate method is suggested to substitute a multiwall nanotube of many layers by a multilayer elastic shell of fewer layers with acceptable relative errors. Especially, the present results show that the predicted increase of the critical axial stress due to an internal radial pressure appears to be in qualitative agreement with some known results for filled singlewall carbon nanotubes obtained by molecular dynamics simulations.

Keywords: Shell; Buckling; Carbon nanotubes

1. Introduction

Carbon nanotubes (CNTs) are the most promising new material and expected to play a pivotal role in nanotechnology (Ball, 2001; Baughman et al., 2002). Mechanical behavior of CNTs, including axially compressed elastic buckling, has been one of recent topics of considerable interest (Treacy et al., 1996; Wong et al., 1997; Poncharal et al., 1999; Yakobson et al., 1996; Falvo et al., 1997; Ru, 2000a,b, 2001a,b). Especially, detailed comparison has shown (Ru, 2000a) that the critical stress and buckling wavelength predicted by isotropic elastic shell model are in good agreement with the results of axially compressed

* Corresponding author. Tel.: +1-780-492-4477; fax: +1-780-492-2200.
E-mail address: c.ru@ualberta.ca (C.Q. Ru).

0020-7683/03/$ - see front matter © 2003 Elsevier Science Ltd. All rights reserved.
doi:10.1016/S0020-7683(03)00213-0

singlewall nanotubes (SWNTs) obtained by molecular dynamics simulations. It is believed that isotropic elastic shell model can be used to catch main features of buckling behavior of SWNTs. On the other hand, axially compressed buckling of multiwall nanotubes (MWNTs) of larger radius-to-thickness ratio has been studied based on a multiple-elastic shell model (Ru, 2000b, 2001a,b), although a comparison is still not available due to the lack of relevant experimental results or molecular dynamics simulations for MWNTs.

Recently, SWNTs (Peters et al., 2000; Venkateswaran et al., 1999; Gaal et al., 2000; Ru, 2000c) and MWNTs (Thomsen et al., 1999; Tang et al., 2000; Venkateswaran et al., 2001; Thomsen and Reich, 2001) under external radial pressure have been the subject of numerous researches. A remarkable phenomenon is the pressure-induced abrupt change of physical properties of SWNTs and MWNTs when the applied pressure reaches a critical value. In an effort to explain these phenomena in terms of pressure-induced elastic buckling, an elastic honeycomb model for SWNT ropes has been developed by Ru (2000c), which leads to a simple critical pressure formula in excellent agreement with known experimental data (Peters et al., 2000; Venkateswaran et al., 1999; Gaal et al., 2000). Furthermore, Wang et al. (2003) have recently studied elastic buckling of individual MWNTs under external radial pressure based on the multiple-elastic shell model (Ru, 2000b, 2001a,b). Wang et al.'s results shown that the predicted critical pressure, about 1 GPa, is in reasonably good agreement with the experimental results (about 1.5 GPa, which, to our best knowledge, is probably the only available experimental data for critical radial pressure of MWNTs) of Tang et al. (2000) for a specific group of MWNTs of about 20 layers. This agreement offers an evidence for the relevance of the multiple-elastic shell model (Ru, 2000b, 2001a,b) to MWNTs, which suggests that the multiple-elastic shell model can be used to study buckling behavior of MWNTs. Here, it should be mentioned that MWNTs under radial internal pressure has been suggested by Thomsen and Reich (2001) as a simplified model for MWNTs filled with some other molecules.

To our knowledge, elastic buckling of CNTs under combined loadings remains an open topic in the literature. Very recently, axially compressed buckling of SWNTs filled with other molecules has been studied by Ni et al. (2002). These authors found that the critical axial strain increases by 10–20% for different filling molecules at low density, and up to 45% for filling molecules at high density. As we mentioned, the role of filling molecules can be modeled approximately by an internal pressure. Although the value of this equivalent internal pressure depends on the filling molecules and the density, and thus cannot be determined exactly, its magnitude can be assumed to be of the order of magnitude of the critical radial external pressure (Thomsen and Reich, 2001) (the latter is about 5% of the critical axial stress for SWNTs (Ru, 2000a)). Therefore, filled SWNTs can be approximately modeled as SWNTs subjected to an internal radial pressure not much higher than 5% of the critical axial stress. Motivated by all of the above ideas, the present work is devoted to a systematic study of axially compressed buckling of MWNTs subjected to an internal or external radial pressure, with an emphasis on new physical phenomena due to combined radial pressure and axial stress. The analysis is based on the multiple-elastic shell model (Ru, 2000b, 2001a,b). According to the radius-to-thickness ratio, multiwall CNTs discussed here are classified into three types: thin, thick, and (almost) solid. In particular, an approximate method is suggested to reduce the problem of a MWNT of many layers to a relatively simple problem of a multilayer elastic shell of fewer layers. The accuracy of this approximate method is demonstrated with examples. Among other results, the present analysis shows that the predicted increase of critical axial stress due to an internal radial pressure is in qualitative agreement with the results for filled CNTs obtained by molecular dynamics simulations (Ni et al., 2002).

2. Basic equations

The elastic-shell models have been effectively applied to SWNTs and MWNTs (Yakobson et al., 1996; Falvo et al., 1997; Ru, 2000a,b, 2001a,b). For MWNTs, a multiple-elastic shell model has been developed by Ru (2000b, 2001a,b), which assumes that each of the concentric nanotubes is described as an individual

elastic shell, and the interlayer friction is negligible between any two adjacent tubes. In the absence of any tangential external force, elastic buckling of a cylindrical shell of radius R is governed by Ru (2000b, 2001a,b), Timoshenko and Gere (1961) and Calladine (1983).

$$D_0\nabla^8 w = \nabla^4 p(x,\theta) + F_x\frac{\partial^2}{\partial x^2}\nabla^4 w + \frac{F_\theta}{R^2}\frac{\partial^2}{\partial\theta^2}\nabla^4 w - \frac{Eh}{R^2}\frac{\partial^4 w}{\partial x^4}, \tag{1}$$

where x and θ are axial coordinate and circumferential angular coordinate, respectively, w is the radial (inward) deflection due to buckling, $p(x,\theta)$ is the net normal (inward) pressure due to buckling, F_x and F_θ are the known uniform axial and circumferential membrane forces prior to buckling, D_0 and h are the effective bending stiffness and thickness of the shell, and E is Young's modulus. Here, the effective bending stiffness D_0 can be independent of the thickness h, and thus not necessarily proportional to h cube.

The present work studies elastic buckling of a MWNT under combined axial stress and radial pressure, as shown in Fig. 1. Applying Eq. (1) to each of all concentric tubes of a MWNT, elastic buckling of a MWNT is governed by the N coupled equations

$$\begin{aligned}
D_1\nabla_1^8 w_1 &= \nabla_1^4 p_{12} + F_x^{(1)}\frac{\partial^2}{\partial x^2}\nabla_1^4 w_1 + \frac{F_\theta^{(1)}}{R_1^2}\frac{\partial^2}{\partial\theta^2}\nabla_1^4 w_1 - \frac{Et_1}{R_1^2}\frac{\partial^4 w_1}{\partial x^4},\\
D_2\nabla_2^8 w_2 &= \nabla_2^4\left[p_{23} - \frac{R_1}{R_2}p_{12}\right] + F_x^{(2)}\frac{\partial^2}{\partial x^2}\nabla_2^4 w_2 + \frac{F_\theta^{(2)}}{R_2^2}\frac{\partial^2}{\partial\theta^2}\nabla_2^4 w_2 - \frac{Et_2}{R_2^2}\frac{\partial^4 w_2}{\partial x^4},\\
&\vdots\\
D_N\nabla_N^8 w_N &= -\frac{R_{N-1}}{R_N}\nabla_N^4 p_{(N-1)N} + F_x^{(N)}\frac{\partial^2}{\partial x^2}\nabla_N^4 w_N + \frac{F_\theta^{(N)}}{R_N^2}\frac{\partial^2}{\partial\theta^2}\nabla_N^4 w_N - \frac{Et_N}{R_N^2}\frac{\partial^4 w_N}{\partial x^4},
\end{aligned} \tag{2}$$

where w_k $(k = 1,2,\ldots,N)$ is the (inward) deflection of the kth tube, D_k and t_k are the bending stiffness and thickness of the kth tube, the subscripts $1,2,\ldots,N$ denote the quantities of the innermost tube, its adjacent tube,... and the outermost tube, respectively, E is Young's modulus of CNTs, R_k is the radius of the kth tube, $F_x^{(k)}$ and $F_\theta^{(k)}$ $(k = 1,2,\ldots,N)$ are the uniform axial and circumferential membrane forces of the kth tube prior to buckling, and

$$\nabla_k^2 = \frac{\partial^2}{\partial x^2} + \frac{1}{R_k^2}\frac{\partial^2}{\partial\theta^2} \quad (k = 1,2,\ldots,N). \tag{3}$$

In addition, $p_{k(k+1)}$ is the (inward) pressure on tube k due to tube $k+1$, $p_{(k+1)k}$ is the (inward) pressure on tube $(k+1)$ due to tube k, and they are related by

$$R_k p_{k(k+1)} = -R_{k+1}p_{(k+1)k} \quad (k = 1,2,\ldots,N). \tag{4}$$

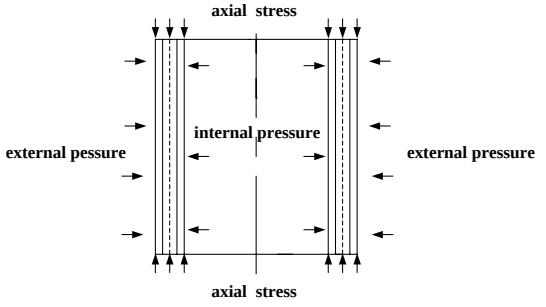

Fig. 1. Axially compressed buckling of a MWNT under radial external or internal pressure.

Here, because the pressures $p_{k(k+1)}$ in (2) is the (inward) pressure exerted on the tube k by the tube $(k+1)$ due to buckling, thus $p_{01}=0$ and $p_{N(N+1)}=0$. In addition, it should be mentioned that the net (inward) pressure for each layer is obtained simply as the sum of the outer (inward) pressure and the inner (inward) pressure. This will not cause any significant error when the radius of each layer is much bigger than its thickness.

Since all nested tubes are originally concentric and the initial interlayer spacing is equal or very close to the equilibrium spacing, the initial van der Waals interaction pressure between any two adjacent tubes of undeformed MWNTs is negligible. When the axial stress and radial pressure are applied, the interlayer spacing changes, and the van der Waals interaction pressure (per unit area) at any point between any two adjacent tubes depends linearly on the difference of the radial deflections at that point. Thus, the pressure $p_{k(k+1)}$ to buckling (see (2)) is related to the deflections of tube k and tube $(k+1)$ due to buckling by

$$p_{12}=c[w_2-w_1], p_{23}=c[w_3-w_2], \ldots, p_{(N-1)N}=c[w_N-w_{N-1}]. \tag{5}$$

Here, the vdW interaction coefficient c can be estimated as the second derivative of the energy–interlayer spacing relation of MWNTs using recent data given by Saito et al. (2001) as

$$c=\frac{320\times \text{erg/cm}^2}{0.16d^2} \quad (d=1.42\times 10^{-8}\ \text{cm}), \tag{6}$$

which are slightly bigger than those used in Ru (2001a,b). Here, because the present analysis is limited to infinitesimal buckling, the coefficient c is calculated at the initial interlayer spacing (about 0.34 nm). The curvature-dependency of the coefficient c is neglected here because it is very small when the innermost radii are much larger than 0.6 nm (Robertson et al., 1992; Gulseren et al., 2002).

Substitution of (5) into (2) leads to N coupled linear equations for N deflections w_k $(k=1,2,\ldots,N)$. The condition for existence of a non-zero solution will determine the critical values for elastic buckling of MWNTs under combined axial stress and radial pressure. To this end, one has to first determine all membrane forces $F_x^{(k)}$ and $F_\theta^{(k)}$ $(k=1,2,\ldots,N)$ prior to buckling.

3. Pre-buckling analysis

Constraints for the ends of cylindrical shell are usually ignored in pre-buckling analysis (Timoshenko and Gere, 1961; Calladine, 1983). As a result, under uniform axial stress and radial external or internal pressure, the axial and circumferential membrane forces $F_x^{(k)}$ and $F_\theta^{(k)}$ $(k=1,2,\ldots,N)$ prior to buckling are some constants. The equilibrium conditions prior to buckling give

$$\sigma_\theta^{(k)}=\frac{F_\theta^{(k)}}{h_k}=-\frac{p_kR_k}{h_k}, \quad \sigma_x^{(k)}=\frac{F_x^{(k)}}{h_k}=\sigma_{\text{axial}} \qquad (k=1,2,\ldots,N), \tag{7}$$

where $\sigma_\theta^{(k)}$ and $\sigma_x^{(k)}$ are the pre-buckling axial and circumferential membrane stresses in the kth tube, p_k is the net (inward) pressure to the kth tube, and σ_{axial} is the axial stress applied to the MWNT. Note that (Hooke's relation)

$$\varepsilon_\theta^{(k)}=\frac{\Delta R_k}{R_k}=\frac{1}{E}(\sigma_\theta^{(k)}-\nu\sigma_x^{(k)}) \quad (k=1,2,\ldots,N), \tag{8}$$

where ΔR_k is the radial (inward) deflection of the kth tube prior to buckling, or the difference between the initial radius R_k and the deformed radius of the kth tube prior to buckling, and ν is Poisson's ratio. Thus, prior to buckling, we have

$$\frac{\Delta R_k}{R_k}=-\frac{1}{E}\left(\frac{p_k\cdot R_k}{h_k}+\nu\cdot\sigma_{\text{axial}}\right) \quad (k=1,2,\ldots,N). \tag{9}$$

For pre-buckling analysis ($k = 2, 3, \ldots, N-1$),

$$\begin{aligned} p_1 &= p_{12} + p_{10} = c(\Delta R_2 - \Delta R_1) - P_{\text{int}}, \\ p_k &= p_{k(k+1)} + p_{k(k-1)} = p_{k(k+1)} - \frac{R_{k-1}}{R_k} \cdot p_{(k-1)k} = c \cdot \left[(\Delta R_{k+1} - \Delta R_k) - \frac{R_{k-1}}{R_k} (\Delta R_k - \Delta R_{k-1}) \right], \\ p_N &= p_{N(N+1)} + p_{N(N-1)} = p_{N(N+1)} - \frac{R_{N-1}}{R_N} P_{(N-1)N} = P_{\text{ext}} - c \frac{R_{N-1}}{R_N} (\Delta R_N - \Delta R_{N-1}), \end{aligned} \tag{10}$$

where P_{int} $(= -p_{10})$ is the applied internal pressure, and P_{ext} $(= p_{N(N+1)})$ is the applied external pressure. Substituting (10) to (8) gives N conditions which allow us to determine ΔR_k $(k = 1, 2, 3, \ldots, N)$. Once these constants are known, all pressure distribution can be determined.

In this paper, according to the radius-to-thickness ratio of MWNTs, we shall classify all MWNTs into the following three typical cases:

(a) thin MWNTs (the innermost radius-to-thickness ratio is larger than five);
(b) thick MWNTs (the innermost radius-to-thickness ratio is around unity);
(c) (almost) solid MWNTs (the innermost radius-to-thickness ratio is smaller than 1/4).

We shall consider six examples shown in Table 1. Obviously, examples 1, 2 are thin MWNTs, examples 4, 5 are thick MWNTs, while example 6 is solid MWNT. In particular, example 3 for SWNTs is included here, as a special case $N = 1$, for a comparison with Ni et al. (2002) which, to our knowledge, is probably the only available result regarding the effect of filling molecules on the critical axial stress of CNTs. As suggested by Thomsen and Reich (2001), the role of filling molecules can be modeled approximately by an internal pressure of the order of magnitude of the critical external pressure. Hence, the results of Ni et al. (2002) offer a chance for us to compare the present model with molecular dynamics simulations.

The distributions of outer pressure $p_{k(k+1)}$ and the net pressure p_k $(k = 1, 2, \ldots, N)$ normalized by the axial stress for three representative examples (1, 4 and 6) are shown in Figs. 2–4 and 5–7 for combined axial stress and external or internal pressure, respectively. In Figs. 2–4, the pressure distribution under combined axial stress and external pressure is given for various external pressure-to-axial stress ratio q_1. It is seen that both the net pressure p_k and the outer pressure $p_{k(k+1)}$ decrease monotonically from the outermost tube to the innermost tube, and are very low for the innermost few tubes of a thick (example 4) or solid (example 6) MWNT. In particular, for thin MWNTs (example 1), the outer pressure is almost linearly distributed, and the net pressure is almost constant. This means that all concentric tubes of a thin MWNT almost equally share the applied external pressure. In this case, as will be shown below, a thin N-wall CNT is approximately equivalent to a single layer elastic shell of the average radius of the MWNT.

In addition, the net pressure p_k and the outer pressure $p_{k(k+1)}$ for combined axial stress and internal pressure are shown in Figs. 5–7 for various internal pressure-to-axial stress ratio q_2. It is seen from Figs. 5–7 that, both the net pressure p_k and the outer pressure $p_{k(k+1)}$ decrease monotonically from the innermost tube

Table 1
The geometrical data for examples of MWNTs

Example	Thin MWNTs		Thick MWNTs			Solid MWNTs
The example number	1	2	3	4	5	6
R_1 (nm)	8.5	18	0.65	2.7	6.5	0.65
R_1/Nt	5.00	6.62	1.9	0.99	1.20	0.24
N	5	8	1	8	16	8

R_1 is the innermost radius of a MWNT, N is the number of layers of the MWNT, and t (=0.34 nm) is the effective thickness of a SWNT.

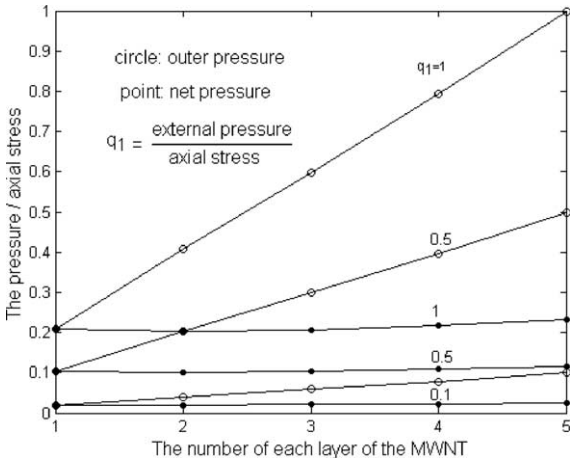

Fig. 2. Pre-buckling pressure distribution under combined axial stress and external pressure (example 1).

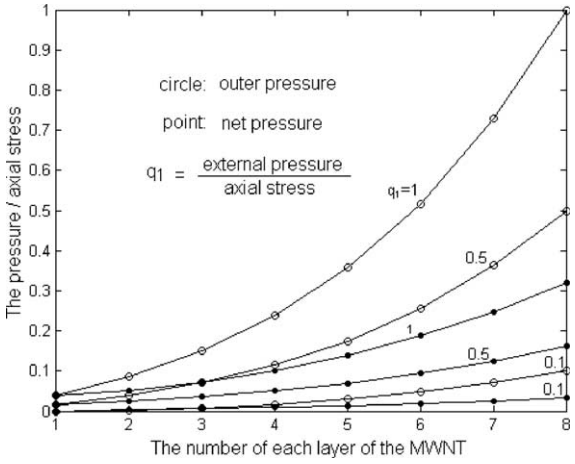

Fig. 3. Pre-buckling pressure distribution under combined axial stress and external pressure (example 4).

to the outermost tube, and are very low for the outermost few tubes of a thick (example 4) or solid (example 6) MWNT. Therefore, the applied internal pressure only significantly affects the innermost few tubes, and has little influence on the pressure distributions of the outermost tubes of thick or solid MWNTs. On the other hand, for thin MWNTs (example 1), it is seen from Fig. 5 that the outer pressure can be considered to be nearly linearly distributed and the net pressure be nearly constant.

4. Buckling analysis

With the known net pressure distribution, we are now able to study elastic buckling of MWNTs under combined axial stress and radial external or internal pressure. Here, we shall consider that the ends of all tubes are simply supported. Thus, the buckling mode is given by

$$w_k = A_k \sin\frac{m\pi}{L}x\cos n\theta \quad (m \geqslant 1), \tag{11}$$

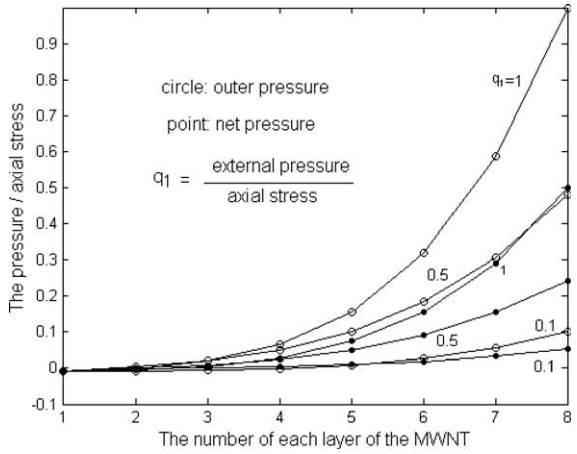

Fig. 4. Pre-buckling pressure distribution under combined axial stress and external pressure (example 6).

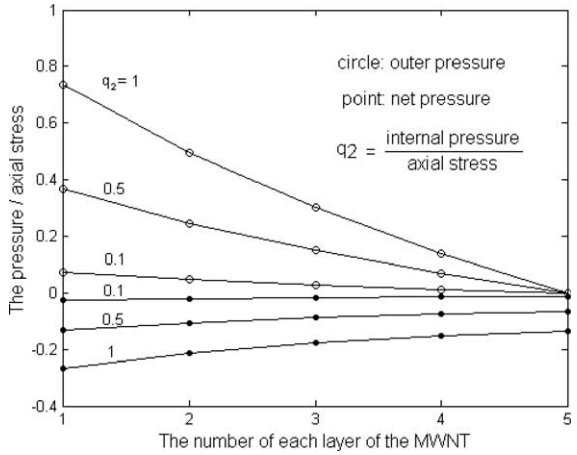

Fig. 5. Pre-buckling pressure distribution under combined axial stress and internal pressure (example 1).

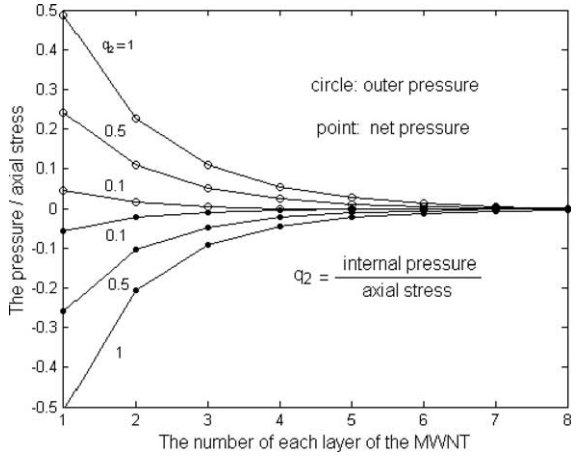

Fig. 6. Pre-buckling pressure distribution under combined axial stress and internal pressure (example 4).

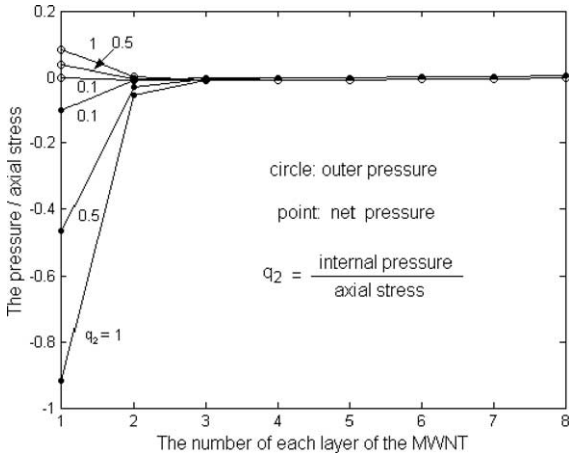

Fig. 7. Pre-buckling pressure distribution under combined axial stress and internal pressure (example 6).

where A_k $(k = 1, 2, \ldots, N)$ are some real coefficients, L is the length of the MWNT, m is the axial half wavenumber, and n is the circumferential wavenumber. Introducing (11), together with the known net pressure distribution (see Section 3), into Eqs. (2) gives

$$
\begin{aligned}
&\left\{ \frac{D}{c}\left[\left(\frac{m\pi}{L}\right)^2+\left(\frac{n}{R_1}\right)^2\right]^4+\left[1+\left(\left(\frac{m\pi}{L}\right)^2 t+\left(-\frac{p_1}{\sigma_{\text{axial}}}\right)\cdot\frac{n^2}{R_1}\right)\cdot\frac{\sigma_{\text{axial}}}{c}\right]\cdot\left[\left(\frac{m\pi}{L}\right)^2+\left(\frac{n}{R_1}\right)^2\right]^2 \right.\\
&\qquad \left. +\frac{Et}{cR_1^2}\left(\frac{m\pi}{L}\right)^4\right\}\cdot A_1+\left\{-\left[\left(\frac{m\pi}{L}\right)^2+\left(\frac{n}{R_1}\right)^2\right]^2\right\}\cdot A_2=0,\\
&\quad\vdots\\
&\left\{-\frac{R_{k-1}}{R_k}\left[\left(\frac{m\pi}{L}\right)^2+\left(\frac{n}{R_k}\right)^2\right]^2\right\}\cdot A_{k-1}+\left\{\frac{D}{c}\left[\left(\frac{m\pi}{L}\right)^2+\left(\frac{n}{R_k}\right)^2\right]^4\right.\\
&\qquad +\left[1+\left(\left(\frac{m\pi}{L}\right)^2 t+\left(-\frac{p_k}{\sigma_{axiial}}\right)\cdot\frac{n^2}{R_k}\right)\cdot\frac{\sigma_{\text{axial}}}{c}+\frac{R_{k-1}}{R_k}\right]\cdot\left[\left(\frac{m\pi}{L}\right)^2+\left(\frac{n}{R_k}\right)^2\right]^2\\
&\qquad \left.+\frac{Et}{cR_k^2}\left(\frac{m\pi}{L}\right)^4\right\}\cdot A_k+\left\{-\left[\left(\frac{m\pi}{L}\right)^2+\left(\frac{n}{R_k}\right)^2\right]^2\right\}\cdot A_{k+1}=0,\\
&\quad\vdots\\
&\left\{-\frac{R_{N-1}}{R_N}\left[\left(\frac{m\pi}{L}\right)^2+\left(\frac{n}{R_N}\right)^2\right]^2\right\}\cdot A_{N-1}+\left\{\frac{D}{c}\left[\left(\frac{m\pi}{L}\right)^2+\left(\frac{n}{R_N}\right)^2\right]^4\right.\\
&\qquad +\left[\left(\left(\frac{m\pi}{L}\right)^2 t+\left(-\frac{p_N}{\sigma_{\text{axial}}}\right)\cdot\frac{n^2}{R_N}\right)\cdot\frac{\sigma_{\text{axial}}}{c}+\frac{R_{N-1}}{R_N}\right]\cdot\left[\left(\frac{m\pi}{L}\right)^2+\left(\frac{n}{R_N}\right)^2\right]^2\\
&\qquad \left.+\frac{Et}{cR_N^2}\left(\frac{m\pi}{L}\right)^4\right\}\cdot A_N=0.
\end{aligned}
\tag{12}
$$

These Eqs. (12) can be written into

$$M(m,n)_{N\times N}\begin{bmatrix} A_1 \\ A_2 \\ \vdots \\ A_N \end{bmatrix} = 0. \tag{13}$$

Thus, the existence condition of a non-zero solution of A_k $(k = 1, 2, \ldots, N)$ is

$$\det M = 0. \tag{14}$$

This condition determines a relationship between the applied axial stress σ_{axial} and (m, n). Throughout the paper, we shall assume that $L = 12R_N$ (the outermost radius), and $v = 0.3$ (Falvo et al., 1997), $D = 0.85$ eV and $Et = 360$ J/m^2 (Yakobson et al., 1996; Ru, 2000a).

4.1. An approximate method for MWNTs of many layers (example 5)

As mentioned before, a thin N-wall CNT can be approximately modeled as a singlelayer elastic shell with the equivalent bending stiffness ND and the thickness Nt (where D and t are effective bending stiffness and thickness of SWNTs). A similar conclusion has been drawn for axially compressed buckling (Ru, 2001a,b) and externally pressured buckling (Wang et al., 2003) of thin MWNTs. Based on these results, an approximate method is suggested here to substitute a (not necessarily thin) MWNT of many layers by a multilayer elastic shell of fewer layers. This simplified method could further improve the effectiveness of the multiple-elastic shell model (Ru, 2000b, 2001a,b) especially when the number N of nested tubes is very large (such as example 5).

To illustrate this approximate method, let us apply it to examples 4 and 5. First, for example 4 consisting of eight layers, let us treat the outermost three layers as a singlelayer shell (the layer IV) with bending stiffness $3D$ and thickness $3t$. Obviously, the radius-to-thickness ratio of this new layer is larger than 5 and thus it can be treated as a thin layer. Next, the following two tubes are treated as another singlelayer shell (the layer III) with bending stiffness $2D$ and thickness $2t$, with the radius-to-thickness ratio larger than 6. Further, the next two tubes are treated as another singlelayer shell (the layer II) with bending stiffness $2D$ and thickness $2t$, with the radius-to-thickness ratio larger than 5. Finally, the innermost layer is treated as a singlelayer elastic shell (the layer I). Thus, the original eight-layer shell (with the layers 1–8) is reduced to a four-layer shell (with the layers I–IV). Eqs. (2) can now be used to this new four-layer shell with: $D_1 = D$, $D_2 = 2D$, $D_3 = 2D$, $D_4 = 3D$, $t_1 = t$, $t_2 = 2t$, $t_3 = 2t$ and $t_4 = 3t$, and the radius and the deflection of each new layer should be understood as its average radius and the deflection of its middle line. In addition, the net pressure distribution stays unchanged, and thus the net pressure for every new layer can be obtained directly from the data shown in Section 3. On the other hand, the vdW interaction pressure on the layer III due to the layer IV (the new outermost layer) is determined by the spacing change between the layer 5 and the layer 6, and is equal to $c(w_6 - w_5)$. Assume that the change of interlayer spacing due to buckling is approximately uniform between the middle lines of the two adjacent new layers (the layer IV and III), thus we have $(w_{\text{IV}} - w_{\text{III}}) = (w_6 - w_5)\times$ (the number of the layers between the two middle lines). Thus, the vdW pressure on the layer III due to the layer IV is $c(w_{\text{IV}} - w_{\text{III}})/2.5$. Similar modification should be made to the vdW interaction pressure between any other adjacent new layers. Here, the interaction pressure between any two adjacent layers within each new layer is an "internal force" for the new layer and this is not accounted as an external pressure. As will be seen later, comparison between the results based on this approximate method with the exact solution for example 4 shows that the relative errors of this method are limited to 10 %.

Table 2
Substitution of a five-layer elastic shell for a MWNT of 16 layers (example 5)

The new layer number	I	II	III	IV	V
k	1	3	3	4	5
h (nm)	0.34	1.02	1.02	1.36	1.70
R_{inner} (nm)	6.5	6.84	7.86	8.88	10.24
R_{inner}/h		6.71	7.71	6.53	6.02

k is the number of concentric tubes of each new layer, h and R_{inner} are thickness and the inner radius of each new layer.

In this paper, we shall apply this approximate method to example 5 of 16 layers. In this case, as shown in Table 2, the outermost five layers are treated as a singlelayer shell with bending stiffness $5D$ and thickness $5t$. Obviously, the radius-to-thickness ratio of this new layer is larger than 6, and thus it can be treated as a thin shell. Next, the next four tubes are treated as another singlelayer shell with bending stiffness $4D$ and thickness $4t$, with the radius-to-thickness ratio larger than 6. Then, the next three tubes will be treated as another singlelayer shell with bending stiffness $3D$ and thickness $3t$, with the radius-to-thickness ratio larger than 7. Further, the next singlelayer shell also consists of three tubes and has bending stiffness $3D$, thickness $3t$, and the radius-to-thickness ratio larger than 7. Finally, the innermost layer is treated as a singlelayer elastic shell. Thus, the original MWNT of 16-layer is reduced to a five-layer shell. In what follows, all results for example 5 will be obtained with this approximate method.

4.2. Pure axial load

First, let us examine elastic buckling of MWNTs under pure axial stress. Prior related works have been essentially limited to SWNTs (Yakobson et al., 1996; Ru, 2000a) and thin MWNTs of larger radius-to-thickness ratio (Ru, 2000b, 2001a,b). Here, instead, we shall consider all three types of MWNTs, including thick and solid MWNTs. The dependency of axial buckling stress on the wavenumbers (m, n) is shown in Figs. 8–12 for five examples (examples 1, 2, 4, 5 and 6) of MWNTs, respectively. An interesting general result is that, similar to classic results of axially compressed buckling of elastic thin shells (Timoshenko and Gere, 1961; Calladine, 1983), the wavenumbers corresponding to the minimum axial stress are not unique for all three types of MWNTs. More precisely, there always is more than one combination of (m, n) which

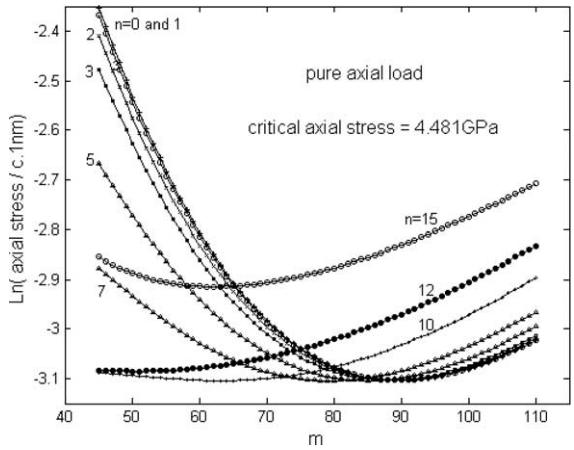

Fig. 8. The dependency of axial stress on the wavenumbers (m, n) (example 1).

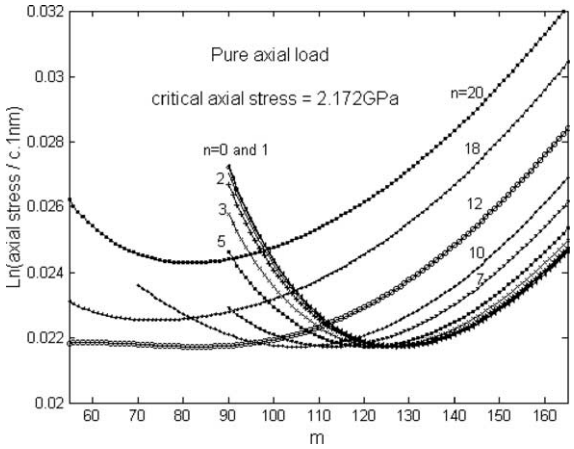

Fig. 9. The dependency of axial stress on the wavenumbers (m, n) (example 2).

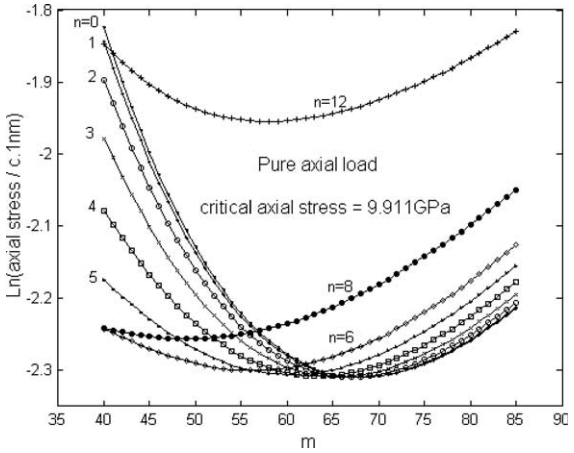

Fig. 10. The dependency of axial stress on the wavenumbers (m, n) (example 4).

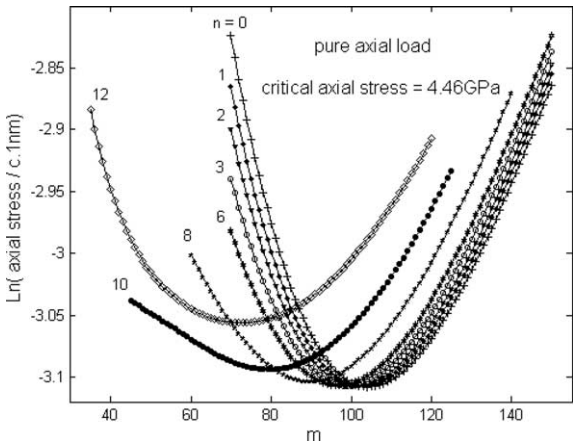

Fig. 11. The dependency of axial stress on the wavenumbers (m, n) (example 5).

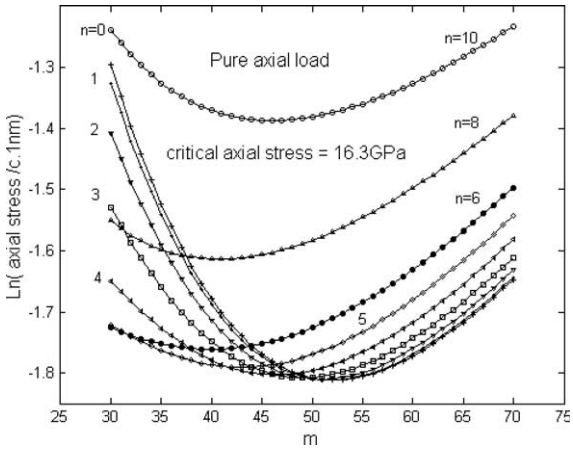

Fig. 12. The dependency of axial stress on the wavenumbers (m, n) (example 6).

corresponds to the same minimum (critical) axial stress. As a result, the wavenumbers of the buckling mode of MWNTs under pure axial stress cannot be determined uniquely.

As mentioned before, many results suggested that a thin MWNT can be approximated by an equivalent singlelayer shell whose effective bending stiffness and thickness are N times the effective bending stiffness and thickness of singlewall CNTs. For the sake of comparison, buckling behavior of singlelayer shells equivalent to two thin MWNTs (examples 1 and 2) in the above sense are shown in Figs. 13 and 14, respectively. Comparison between Figs. 8 and 13, and between Figs. 9 and 14, indicates that thin N-wall CNTs can indeed be well approximated by a singlelayer elastic shell with the equivalent bending stiffness ND and the thickness Nt. In fact, both the critical axial stress and the associated wavenumbers (m, n) are almost the same for thin MWNTs and their equivalent singlelayer shells. For example, the critical axial stress for example 1 by the singlelayer shell model is 4.480 GPa, which is very close to the exact value 4.481 GPa shown in Fig. 8. Similarly, the critical axial stress for example 2 by the singlelayer shell model is 2.186 GPa, very close to the exact value 2.172 GPa. This offers a numerical confirmation of the analytical results

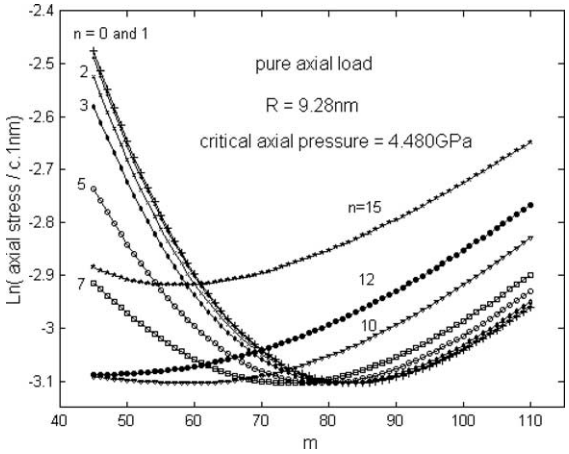

Fig. 13. The dependency of axial stress on the wavenumbers (m, n) (singlelayer shell equivalent to example 1).

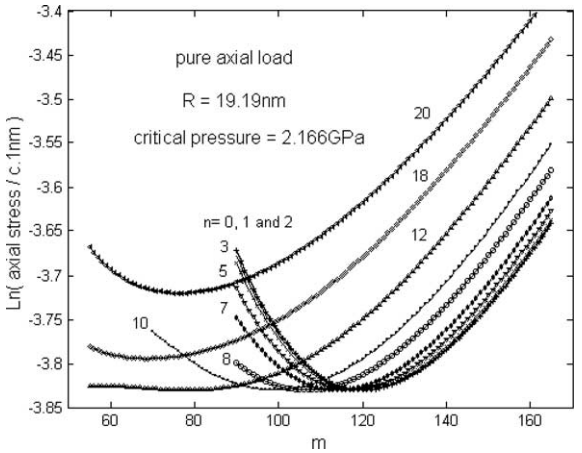

Fig. 14. The dependency of axial stress on the wavenumbers (m, n) (singlelayer shell equivalent to example 2).

Table 3
Critical axial stress for thick or solid MWNTs (examples 4–6) with comparison to the critical axial stress of a related SWNT

Example	Thick MWNTs		Solid MWNT
Example number	4	5	6
σ_{MWNT} (GPa)	9.91	4.46	16.30
σ_{inner} (GPa)	15.40	6.40	64.00
σ_{outer} (GPa)	8.18	3.58	13.72

σ_{MWNT} is the critical axial stress for a MWNT under axial stress, and σ_{inner} and σ_{outer} are critical axial stresses for related SWNTs with the innermost radius or outermost radius of the MWNT.

of Ru (2001b) for thin MWNTs. In particular, this means that the critical axial stress of a thin MWNT is approximately equal to the critical axial stress of a SWNT of the average radius of the MWNT, as stated in Ru (2001b).

On the other hand, the critical axial stresses for three thick or solid MWNTs (examples 4, 5, and 6) are summarized in Table 3, with a comparison to the critical axial stress of a SWNT whose radius is equal to the innermost or the outermost radius of the MWNT. For these examples, the critical axial stress for MWNT is bounded, from above and from below, respectively, by the critical axial stress of a SWNT of the innermost radius of the MWNT, and the critical axial stress of a SWNT of the outermost radius of the MWNT. Here, the results for example 5 of 16 layers are obtained with the approximate method, as shown in Table 2. In particular, for example 4, the critical axial stress based on this approximate method is 9.99 GPa, in good agreement with the exact value 9.91 GPa obtained by the exact eight-layer model, see Table 4.

4.3. Axial stress combined with an internal pressure

Now, let us consider the combined axial stress and internal pressure. One of main results for elastic singlelayer shells under combined axial stress and internal pressure (Timoshenko and Gere, 1961; Calladine, 1983) is that the internal pressure has no effect on axisymmetric buckling mode, but has a significant effect on non-axisymmetric buckling modes. First, for SWNTs, it has been argued (Ru, 2000a) that, due to some unidentified reasons (such as non-axisymmetric atomic structure of SWNT), the actual buckling mode of SWNTs under pure axial stress is non-axisymmetric, and can be approximately determined by the

Table 4
Comparison between exact results for example 4 and results obtained by the approximate method

Loading condition		Pure axial stress	Combined axial stress and external pressure ($q_2 = 0$)			
			$q_1 = 0.01$	$q_1 = 0.05$	$q_1 = 0.1$	$q_1 = 0.5$
Critical axial stress (GPa)	Exact solution	9.91	7.74	1.91	0.99	0.20
	Approximate solution	9.99	8.39	2.01	1.03	0.21
Relative error		0.8%	8.48%	5.07%	4.56%	4.14%

q_1 and q_2 are the external pressure-to-axial stress ratio and the internal pressure-to-axial stress ratio, respectively.

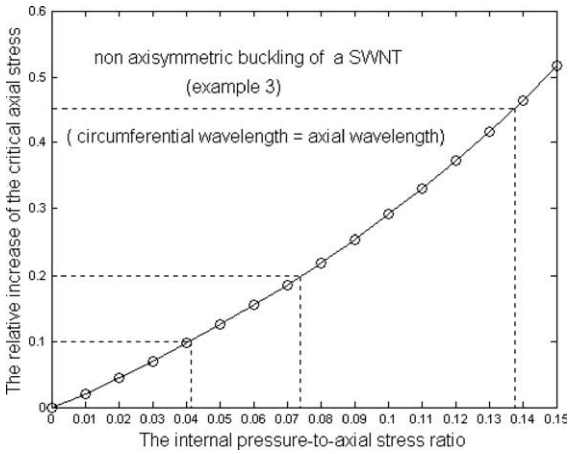

Fig. 15. The effect of an internal pressure on the critical axial stress of SWNTs.

condition that the circumferential wavelength is equal to the axial wavelength. Based on this assumption, the relative change of the critical axial stress for example 3 (a SWNT of diameter 1.3 nm) due to an internal pressure is shown in Fig. 15, as a function of the internal pressure-to-axial stress ratio. It is seen from Fig. 15 that the critical axial stress increases 10%, 20%, and 45% when the internal pressure-to-axial stress ratio is around 0.04, 0.07 and 0.14, respectively. Therefore, the relative increase of the critical axial stress due to filling molecules observed by Ni et al. (2002), which is about 10–20% at low density or 45% at high density, could be explained by an equivalent internal pressure about 5% or 14% of the critical axial stress (or equivalently, by an equivalent internal pressure which is about the critical external pressure or 2–3 times the critical external pressure). Since the internal pressure due to filling molecules can be reasonably assumed to be of the order of magnitude of the critical external pressure (Thomsen and Reich, 2001; Wang et al., 2003), the present theoretical results appear to be in qualitative agreement with Ni et al.'s results obtained by molecular dynamics simulations.

For other three representative examples (1, 4 and 6) of MWNTs, we calculated the minimum axial stress as function of the circumferential wavenumber n, for various internal pressure-to-axial stress ratios. These results are shown in Figs. 16–18 for examples 1, 4 and 6, respectively. It is seen from that the internal pressure has no effect on the axisymmetirc buckling mode ($n = 0$), but significantly promotes the critical axial stress for non-axisymmetric modes. In particular, for non-axisymmetric modes, the effect of internal pressure on the critical axial stress is strong for thin MWNTs (Fig. 16), moderate for thick MWNTs (Fig. 17), and negligible for solid MWNTs (Fig. 18). We noticed that the last conclusion is different from the

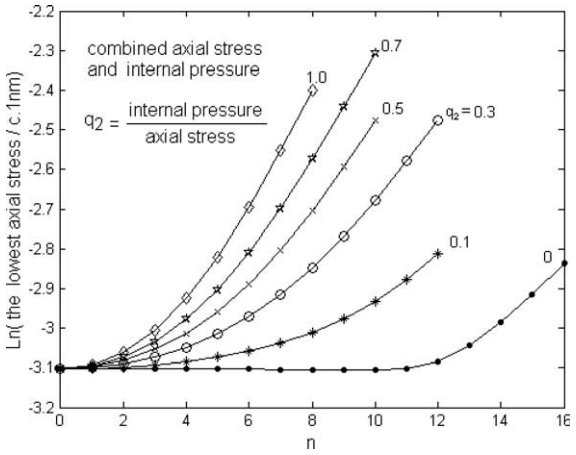

Fig. 16. The effect of an internal pressure on the critical axial stress for various circumferential wavenumber (example 1).

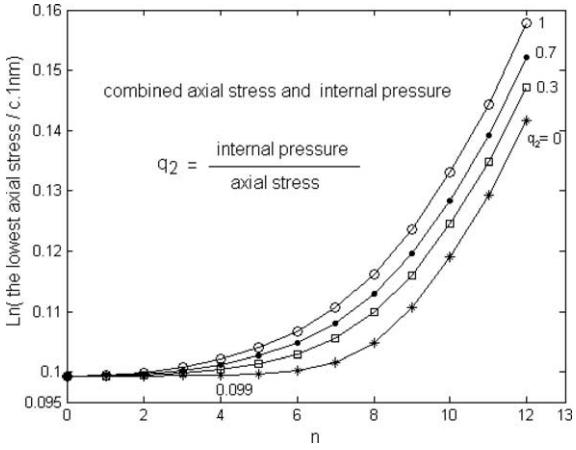

Fig. 17. The effect of an internal pressure on the critical axial stress for various circumferential wavenumber (example 4).

results of (Wang et al., 2003) for combined internal and external pressures (without axial stress) where the internal pressure has a moderate effect on the critical external pressure even for solid MWNTs.

4.4. Axial stress combined with an external pressure

Finally, let us examine elastic buckling of MWNTs under combined axial stress and external pressure. Here we consider all examples 1–6, as well as an additional thin SWNT of radius 5.3 nm. The critical axial stress (under pure axial stress) for these seven examples is 4.481, 2.172, 63.962, 9.911, 4.460, 16.300 and 8.153 GPa, and the critical external pressure (under pure external pressure) is 0.0083, 0.0021, 2.098, 0.102, 0.0297, 1.8805 and 0.0093 GPa, respectively. These critical axial stresses and critical external pressures are obtained by following the procedures demonstrated in Sections 3 and 4 of the present paper and Wang et al. (2003). Two main results for elastic thin shells under combined axial stress and external pressure (Timoshenko and Gere, 1961; Calladine, 1983) are that (1) the buckling mode can be determined uniquely and is

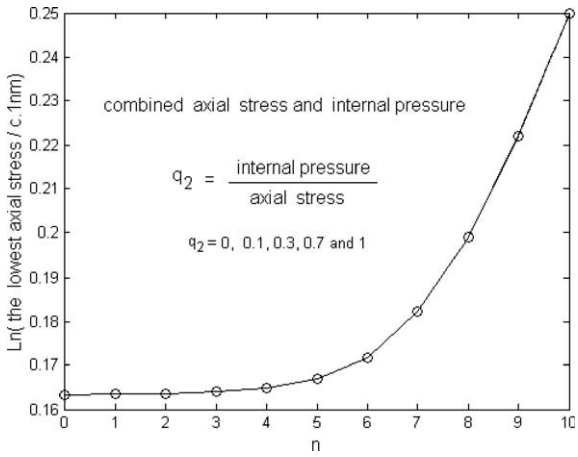

Fig. 18. The effect of an internal pressure on the critical axial stress for various circumferential wavenumber (example 6).

characterized by $m = 1$; (2) the critical condition expressed by a relation between the axial stress and the external pressure is nearly linear. For all examples discussed here, the conclusion that the buckling mode can be determined uniquely remains true, although the buckling mode is not always characterized by $m = 1$. To examine the interaction between the axial stress and external pressure, the critical values of the axial stress and external pressure are calculated with various external pressure-to-axial stress ratios, and the critical condition given in terms of the two critical values, together with the corresponding wavenumbers (m, n), is shown in Figs. 19 and 20 for SWNTs (example 3) and MWNTs (all other examples), respectively. In particular, when the external pressure-to-axial stress ratio is equal to 0.01, 0.05, 0.1 and 0.5, the critical axial stress obtained by the approximate method for example 4 is 8.39, 2.01, 1.03 and 0.21 GPa, respectively, which are in good agreement with the exact result 7.74, 1.91, 0.99 and 0.20 GPa (see Table 4). Therefore, it is expected that the approximate method suggested here can be used to reduce the number of layers of MWNTs without substantial relative errors.

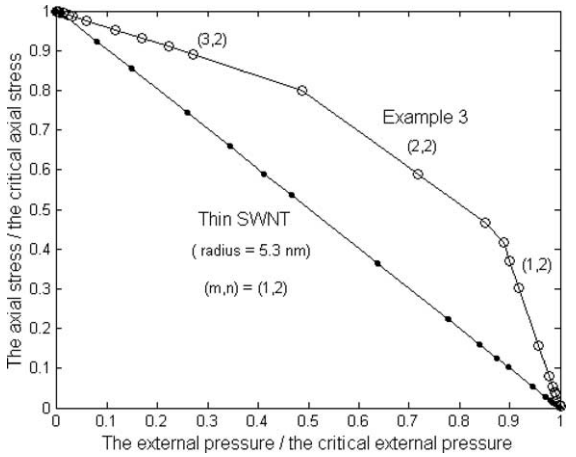

Fig. 19. The critical condition for SWNTs under combined axial stress and external pressure (example 3).

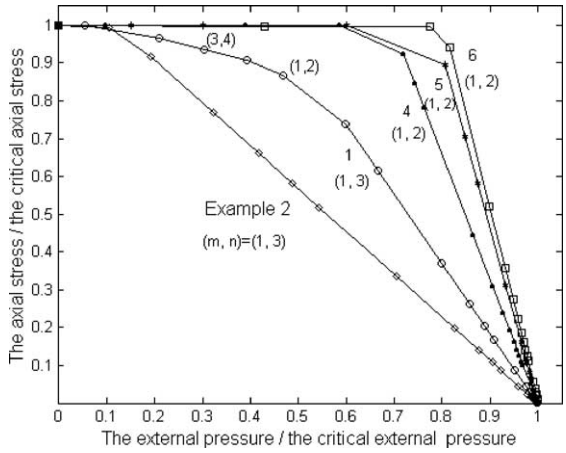

Fig. 20. The critical condition for MWNTs under combined axial stress and external pressure (examples 1, 2, 4, 5 and 6).

It is seen from Figs. 19 and 20 that, the critical condition as a relation between the axial stress and the external pressure is apparently nonlinear for all six examples given in Table 1. This discrepancy with the classic results of elastic thin shells is due to the fact that the radius-to-thickness ratio for these examples is too small compared to that of conventional elastic thin shells (Timoshenko and Gere, 1961; Calladine, 1983). In other words, the critical condition is expected to be nearly linear when the radius-to-thickness ratio of CNTs is sufficiently large. In fact, the example of SWNT of radius 5.3 nm shown in Fig. 19 confirms that the critical condition is indeed nearly linear, because of the sufficient large ratio-to-thickness ratio.

5. Conclusions

This paper gives a systematic analysis of axially compressed buckling of individual multiwall CNTs subjected to radial internal or external pressure. According to their radius-to-thickness ratios, the multiwall CNTs discussed here are classified into three types: thin, thick, and (almost) solid. Our main results are summarized as follows:

(1) A thin N-wall nanotube (defined by the radius-to-thickness ratio larger than 5) can be approximately modeled as a singlelayer elastic shell whose effective bending stiffness and thickness are N times the effective bending stiffness and thickness of singlewall carbon nanotubes. Based on this result and those previously obtained in Ru (2001b) and Wang et al. (2003), an approximate method is suggested to substitute a MWNT of many layers by a multilayer elastic shell of fewer layers. The effectiveness and accuracy of this approximate method are demonstrated with examples. This approximate method could further improve the effectiveness of the multiple-elastic shell model developed in Ru (2000b, 2001a,b) and Wang et al. (2003) especially for MWNTs of large number of layers.
(2) *Pure axial stress*. There always is more than one combination of the axial and circumferential wavenumbers of the buckling mode which corresponds to the same minimum axial stress. On the other hand, the critical axial stress of a thin MWNT is approximately equal to the critical axial stress of a SWNT of the average radius of the MWNT, while the critical axial stress of a thick or solid MWNT is bounded, from above and from below, respectively, by the critical axial stress of a SWNT of the innermost radius of the MWNT, and the critical axial stress of a SWNT of the outermost radius of the MWNT.

(3) *Combined axial stress and internal pressure*. The internal pressure has a significant effect on the critical axial stress for non-axisymmetric modes for both SWNTs and MWNTs discussed here, while it has no effect on the axisymmetirc buckling mode ($n = 0$). As a result, in the absence of any other factor which makes axisymmetric mode prohibited, the critical axial stress could be determined by the axisymmetric mode ($n = 0$). In addition, for non-axisymmetric modes, the effect of internal pressure on the critical axial stress is strong for thin MWNTs, moderate for thick MWNTs, and negligible for solid MWNTs. In particular, the present results for a special case of SWNTs appear to be in qualitative agreement with Ni et al.'s results (Ni et al., 2002) obtained by molecular dynamics simulations.

(4) *Combined axial stress and external pressure*. The buckling mode can be determined uniquely in this case, although it is not always characterized by $m = 1$. The critical condition, expressed as a relation between the axial stress and the external pressure, is strongly nonlinear for all examples. The discrepancy between this nonlinear relation and the well-known nearly linear relation for elastic thin shells (Timoshenko and Gere, 1961; Calladine, 1983) is due to the fact that the radius-to-thickness ratio for the present examples is too small compared to that of conventional elastic thin shells. Indeed, as shown in the paper, the nonlinear relation reduces to a nearly linear one when the radius-to-thickness ratio is sufficiently large.

These results, together with Ru (2000a) and Wang et al. (2003), show convincingly that elastic shell model can be used to describe overall mechanical behavior of CNTs with characteristic length much larger than the C–C bond length (about 0.14 nm) of CNTs. On the other hand, we would like to comment that elastic shell model would be questionable for highly localized deformation with very small characteristic length comparable to the C–C bond length of CNTs, such as cracks or local buckling of very small wavelength.

Acknowledgement

The financial support of the Natural Science and Engineering Research Council of Canada (NSERC) is gratefully acknowledged.

References

Ball, P., 2001. Roll up for the revolution. Nature 414, 142–144.

Baughman, R.H., Zakhidov, A.A., de Heer, W.A., 2002. Carbon nanotubes—the route toward applications. Science 297, 787–792.

Calladine, C.R., 1983. Theory of Shell Structures. Cambridge University Press, Cambridge.

Falvo, M.R., Clary, G.J., Taylor, R.M., Chi, V., Brooks, F.P., Washburn, S., Superfine, R., 1997. Bending and buckling of carbon nanotubes under large strain. Nature 389, 582–584.

Gaal, R., Salvetat, J.P., Forro, L., 2000. Pressure dependence of the resistivity of single-wall carbon nanotube ropes. Phys. Rev. B 61, 7320–7323.

Gulseren, O., Yildirim, T., Ciraci, S., 2002. Systematic ab initio study of curvature effects in carbon nanotubes. Phys. Rev. B 65, 153405–153408.

Ni, B., Sinnott, S.B., Mikulski, P.T., Harrison, J.A., 2002. Compression of carbon nanotubes filled with C_{60}, CH_4, or Ne: predictions from molecular dynamics simulations. Phys. Rev. Lett. 88, 205505-1–205505-4.

Peters, M.J., Mcneil, L.E., Lu, J.P., Kahn, D., 2000. Structure phase transition in carbon nanotube bundles under pressure. Phys. Rev. B 61, 5939–5944.

Poncharal, P., Wang, Z.L., Ugarte, D., de Heer, W.A., 1999. Electrostatic deflections and electromechanical resonances of carbon nanotubes. Science 283, 1513–1516.

Ru, C.Q., 2000a. Effective bending stiffness of carbon nanotubes. Phys. Rev. B 62, 9973–9976.

Ru, C.Q., 2000b. Effect of van der Waals forces on axial buckling of a doublewall carbon nanotube. J. Appl. Phys. 87, 7227–7231.

Ru, C.Q., 2000c. Elastic buckling of singlewalled carbon nanotube ropes under high pressure. Phys. Rev. B 62, 10405–10408.

Ru, C.Q., 2001a. Axially compressed buckling of a doublewalled carbon nanotube embedded in an elastic medium. J. Mech. Phys. Solids 49, 1265–1279.

Ru, C.Q., 2001b. Degraded axial buckling strain of multiwalled carbon nanotubes due to interlayer slips. J. Appl. Phys. 89, 3426–3433.

Robertson, D.H., Brenner, D.W., Mintmire, J.W., 1992. Energrtics of nanoscale graphitic tubules. Phys. Rev. B 45, 12592–12595.

Saito, R., Matsuo, R., Kimura, T., Dresselhaus, G., Dresselhaus, M.S., 2001. Anomalous potential barrier of double-wall carbon nanotube. Chem. Phys. Lett. 348, 187–193.

Tang, D.S., Bao, Z.X., Wang, L.J., Chen, L.C., Sun, L.F., Liu, Z.Q., Zhou, W.Y., Xie, S.S., 2000. The electrical behavior of carbon nanotubes under high pressure. J. Phys. Chem. Solids 61, 1175–1178.

Thomsen, C., Reich, S., 2001. The pressure dependence of the high-energy Raman Modes in empty and filled multiwalled carbon nanotubes. Phys. Status Solidi (b) 225, R18–R19.

Thomsen, C., Reich, S., Jantoljak, H., Loa, I., Syassen, K., Burghard, M., Dueberg, G.S., Rothet, S., 1999. Raman spectroscopy on single- and multi-walled nanotubes under high pressure. Appl. Phys. A 69, 309–312.

Timoshenko, S.P., Gere, J.M., 1961. Theory of Elastic Stability. McGraw-Hill, New York.

Treacy, M.M.J., Ebbesen, T.W., Gibson, J.M., 1996. Exceptionally high Young's modulus observed for individual carbon nanotubes. Nature 381, 678–680.

Venkateswaran, U.D., Brandsen, E.A., Schlecht, U., Rao, A.M., Richter, E., Loa, I., Syassen, K., Eklund, P.C., 2001. High pressure studies of the Raman-Active phonons in carbon nanotube. Phys. Status Solidi (b) 223, 225–236.

Venkateswaran, U.D., Rao, A.M., Richter, E., Menon, M., Rinzler, A., Smalley, R.E., Eklund, P.C., 1999. Probing the single-wall carbon nanotube bundle: Raman scattering under high pressure. Phys. Rev. B 59, 10928–10934.

Wang, C.Y., Ru, C.Q., Mioduchowskil, A., 2003. Elastic buckling of multiwall carbon nanotubes under high pressure. J. Nanosci. Nanotechnol. 3, 199–208.

Wong, E.W., Sheehan, P.E., Lieber, C.M., 1997. Nanobeam mechanics: elasticity, strength, and toughness of nanorods and nanotubes. Science 277, 1971–1975.

Yakobson, B.I., Brabec, C.J., Bernholc, J., 1996. Nanomechanics of carbon tubes: instabilities beyond linear response. Phys. Rev. Lett. 76, 2511–2514.